IEEE Access
Multidisciplinary Rapid Review Open Access Journal

Received 15 July 2022, accepted 16 August 2022, date of publication 19 August 2022, date of current version 26 August 2022.

Digital Object Identifier 10.1109/ACCESS.2022.3200372

RESEARCH ARTICLE

MIMO Hybrid PD-SCMA NOMA Uplink Transceiver System

SIMON CHEGE, (Member, IEEE), AND TOM WALINGO, (Member, IEEE)
Centre for Radio Access and Rural Technologies (CRART), University of KwaZulu–Natal, Durban 4041, South Africa

Corresponding author: Simon Chege (219085519@stu.ukzn.ac.za)

This work was supported by the Centre for Radio Access and Rural Technologies (CRART), University of KwaZulu Natal.

ABSTRACT The application of multiple-input multiple-output (MIMO) on power domain sparse code multiple access (PD-SCMA) systems would enhance their performance by increasing the multiplexing and diversity gains. However, this is at a cost of increased detection complexity, as more users and antennas are deployed. This work develops and investigates the performance of spatial multiplexing MIMO based hybrid PD-SCMA system (M-PD-SCMA) transceiver on an uplink heterogeneous network over Rayleigh flat-fading channels. The aim is to strike a balance on the number of antennas and capacity/spectral efficiency. A low complex modified iterative joint multi-user detector employing expectation propagation algorithm (EPA) and successive interference cancellation (SIC) is proposed for the uplink system. The system capacity and outage robustness of the proposed transceiver in imperfect channels is evaluated and the bit error rate (BER) performance analysed. The link-level simulation results demonstrate that M-PD-SCMA achieves performance benchmark with PD-SCMA schemes. The proposed receiver achieves guaranteed BER performance with an increase in the number of transmit and receive antennas. Besides, the results highlight the impact of the codebook size, number of layers and power level distinctiveness on the outage bounds at each receive antenna at different SNR levels. Thus, the feasibility of an M-PD-SCMA system is validated.

INDEX TERMS PD-SCMA, MIMO, receiver complexity, expectation propagation, NOMA.

I. INTRODUCTION

THE merits and demerits of the evolution of non-orthogonal multiple access (NOMA) schemes from power domain NOMA (PD-NOMA) [1], sparse code multiple access (SCMA) [2], to the hybrid NOMA schemes [3], [4], [5], [6], [7], [8], [9] and their applications in current communication networks have been well investigated. This evolution is fueled by the demand for highly reliable, lower end-to-end latency, spectrally efficient and high data rate multiple access schemes.

To enhance the NOMA experience in advancing efficient spectrum access and latency reduction in Internet of Things (IoT) and smart devices, hybrid NOMA techniques are emerging. A hybrid NOMA proposed in [3] clusters users in small path loss (strong) and large path loss (weak) groups. In [4], sum rate and outage expressions of hybrid NOMA schemes namely, hybrid NOMA-OMA, NOMA Space shift keying (NOMA-SSK) and Successive user relaying cooperative NOMA (SR-NOMA) are derived. The authors observe better performance with NOMA-SSK compared to the other discussed schemes. A hybrid NOMA for ultra dense networks of massive Machine Type Communication (mMTC) deployment is proposed in [5] and its area spectral efficiency compared with pure OMA. Authors in [6] optimize the resource allocation (RA) using bipartite graph and swap matching for an energy efficient hybrid NOMA-OMA system. In [7], a power domain sparse code non-orthogonal multiple access (PD-SCMA) that fuses PD-NOMA and SCMA on a heterogeneous uplink multi-tier network (HetNet) consisting of small cell user equipment's (SUEs) and the macro user equipment's (MUEs) is proposed. The hybrid technology thrives in its ability to connect multiple users in a limited resource scenario by employing hybrid RA schemes at the transmitter. Further, the multiplexing capacity of the hybrid NOMA is investigated in [8]. Authors in [9] propose a joint power and code-domain NOMA for a downlink system. Preliminarily, hybrid NOMA is feasible and can meet the performance requirements of B5G systems.

The associate editor coordinating the review of this manuscript and approving it for publication was Jiankang Zhang.

Multiple-input multiple-output (MIMO) technologies have greatly improved throughput in communication systems. Based upon three key concepts of spatial diversity, spatial multiplexing, and beamforming, MIMO technology application gained traction owing to its gains in system throughput enhancement [10]. Moreover, the integration of MIMO for improving the capacity of NOMA systems is being embraced [11]. In [12], authors investigate MIMO performance with multiple clustered users and analytically proves the superiority of MIMO-NOMA sum channel and ergodic capacity over MIMO-OMA. A robust MIMO-NOMA with low complexity and capacity-approaching solution is proposed in [13] and its performance is validated in practical settings i.e.,varying system loads, iteration numbers, code lengths, fast/block fading, and imperfect channel estimation. Further, MIMO-NOMA finds applications in small packet transmissions in Internet of Things (IoT) users where users have diversified Quality of Service (QoS) requirements [14]. Authors in [15] investigate performance of an indoor 2×2 MIMO-based multi-user visible light communication (VLC) systems. By proposing a normalized gain difference power allocation (NGDPA), the achieved sum-rate is significantly improved.

For enhanced throughput, integration of SCMA with MIMO technologies is an active research area [16], [17], [18], [19], [20], [21], [22]. In [16], diversity and multiplexing based MIMO schemes for uplink SCMA system are investigated. For the multiple access channels (MAC), the receive antennas installed at the base station (BS) give rise to larger diversity order and hence may be used for supporting more users with multiple access gain. By applying Vertical Bell Labs Layered Space Time (V-BLAST) Coding and Space Time Block Coding (STBC) in uplink and downlink respectively, authors in [17] demonstrate improved spectral performance through integration of MIMO and SCMA. Similarly, MIMO-SCMA in [18] demonstrates that system capacity can be preserved with lower number of antennas thanks to the overload in SCMA. In [19], the proposed spatial modulation SCMA (SM-SCMA) scheme employing low complexity joint-message passing algorithm (MPA) based on the principle of the maximum a posterior probability and the simplified factor graph, achieves an improved BER performance. Authors in [20] and [21] investigate the combined downlink detection of MIMO based SCMA for a near-optimal BER performance and notable reduced complexity. Infact, [22] investigates MIMO–SCMA performance with various overload scenarios under Rayleigh and AWGN channel models.

Though the design and application of MIMO based NOMA technologies is still in its early stages, the modelling and performance investigation of multiple antenna based hybrid NOMA schemes is more scarce but gaining traction. In [23], the uplink channel throughput performance of a proposed novel multiple-antenna hybrid-domain NOMA (MA-HD-NOMA) scheme is studied. Similar RA schemes as [3] are employed and a performance comparison made with MIMO based PD-NOMA and SCMA conventional schemes. Employing multiple transmitter and receive antennas in hybrid NOMA schemes could lead to improving on the benefits of the hybrid system in throughput, capacity and diversity. However, this is fraught with the challenges of multiplexing at the transmitter and surging complexity at the receiver as the number of users and antennas grows. Inspired by [20] and [21], the main contribution of this work is the development and integration of MIMO schemes on a hybrid PD-SCMA (M-PD-SCMA) uplink system. We draw the motivation on M-PD-SCMA in the need for minimized number of antennas while preserving the system capacity thanks to the overload in PD-SCMA. We alleviate the integration challenges by employing spatial multiplexing (SM) based MIMO scheme at the transmitter where each transmit antenna at each layer transmits an independent SCMA user codeword.

The hybrid MIMO-NOMA, and in particular, MIMO-SCMA schemes exhibit high detection complexity challenges. Though maximum likelihood (ML) offers optimal performance, the complexity grows exponentially with both the number of the antennas and user equipments (UEs). Owing to their sparsity, the MPA proposed in [20] for detection in MIMO-SCMA can achieve a near-optimal performance. However, MPA's complexity increases exponentially with the codebook size and the degree of symbol superposition on a given resource element (RE). The complexity order becomes more surging for PD-SCMA with increased number of superposed users in power domain in each codebook that require successive interference cancellation (SIC) detection.

At the code domain, several simplified MPA detectors are proposed such as partial-decoding MPA (PD-MPA) [24] that eliminates redundant combinations at resource nodes and the partially active MPA [25] that uses a sliding window to determine which users stay active or silent, both aimed at minimizing the complexity order. Nonetheless, the complexity order exhibited is still exponential. In [26], the expectation propagation algorithm (EPA) is proposed for MIMO-SCMA. Authors in [27] and [28] propose EPA based on the approximation of the real distribution as a Gaussian distribution and obtains the posterior probability through multiple iterations along the factor graph in an SCMA system. Inspired by [27], [28], and [29], this work implements a modified EPA on the code-domain. Differently, the modified EPA develops an extended SM based factor graph for the M-PD-SCMA besides adopting a different message passing on the function node (FN) side. To accelerate the convergence, we adopt a new initialization method on the receiver algorithm.

In summary, this work demonstrates the feasibility of an uplink MIMO based hybrid PD-SCMA transceiver in HetNet and investigates its performance over Rayleigh flat-fading stochastic channel model. The work features the following;

- At the transmitter, a MIMO based uplink PD-SCMA with SUEs and MUEs superimposed in the multi-antenna layers in an imperfect channel is proposed. The choice of spatial multiplexing is informed due to its

TABLE 1. Notation.

Notation	Meaning	Notation	Meaning
$\mathbf{x}$	Coded signal vector	N_t	Transmit antennas
M	Codebook size	N_r	Receive antennas
J	No. of SUEs in a SBS	V	MUEs multiplexed in a Layer
F	No. of SBSs	U	Total MUEs in the system
L	No. of layers	CB	Available codebooks
K	Resource elements (REs)	P	Power vector
$\mathbf{y}$	The received signal vector	$\mathbf{z}$	The complex AWGN vector
$\mathbf{h}$	Channel fading gains	λ	Overloading factor
d_f	No. of layers per RE	d_v	No. of REs per layer

low complexity multiplexing at the transmitter where each transmit antenna at each layer can be configured to transmit an independent SCMA UE codeword.

- At the receiver, a joint MUD employing a modified EPA for the code-domain and SIC for the power domain detection is proposed. By adjusting the initialization method and adapting a new design of message passing between the nodes, the modified EPA exhibits a reduced complexity order and enhanced convergence.
- The BER, system capacity, outage and complexity performance of the M-PD-SCMA system is analysed. The investigation leads to the following deductions; 1). The BER performance is dependent on the number of transceiver antennas, 2). the system capacity references PD-SCMA capacity when system's point of operation is within the multiplexing bounds investigated in [8], 3). the outage bounds closely follow the codebook size, number of layers and power level distinctiveness at different SNR levels and 4). although the overall M-PD-SCMA system complexity surpasses other NOMA schemes, the joint receiver exhibits significantly reduced complexity. The feasibility of an M-PD-SCMA system is thus validated.

A. NOTATION

We denote by x, $\mathbf{x}$, $\mathbf{X}$ and $\mathcal{X}$ a scalar, vector, matrix and set respectively. A set of $M-$ary numbers is denoted by $\mathbb{M}$. What's more, $\mathbf{x}^T$ and $diag(\mathbf{x})$ represent the transpose and diagonal matrix respectively. Besides, $diag(\mathbf{X})$ is a vector of the diagonal elements of matrix $\mathbf{X}$. The summary list of all notations and variables is given in Table 1.

II. MIMO-NOMA SYSTEMS

The integration of MIMO techniques in NOMA systems needs careful attention due to design optimization challenges of beam forming, power allocation, user clustering, and SIC ordering, either jointly or partially, under some performance metric [11]. The application is based on the multiplexing of different user equipments (UEs) on the RE. The structure and use of the RE in NOMA systems can be found in [30] and [31].

A. MULTI-ANTENNA PD-NOMA SYSTEM

At the transmitter, uplink UEs, each equipped with N_t antennas and different channel gains superimpose their signals and transmit simultaneously to communicate with the BS equipped with N_r antennas. Denote as d_v and d_f, the number of accessible REs per UE and the number of UEs that can utilize a RE respectively. In PD-NOMA, each user utilizes only one RE, i.e., $d_v = 1$, and each RE can be accessed by more than one UE, i.e., $d_f \geq 1$. Assuming the transmission is synchronized, the received signal at the n_r-th receiver antenna is given as

$$\mathbf{y}^{n_r} = \sum_{n_t=1}^{N_t} \sum_{i=1}^{d_f} diag(\mathbf{h}_i^{n_t,n_r})\mathbf{x}_i^{n_t} + \mathbf{z}^{n_r} \tag{1}$$

The channel vector $\mathbf{h}_i^{n_t,n_r} = \left[h_{i,UE_1}^{n_t,n_r} h_{i,UE_2}^{n_t,n_r}, \cdots h_{i,UE_V}^{n_t,n_r}\right]^T$ while $\mathbf{x}_i^{n_t} = \left[x_{i,UE}^{n_t} x_{i,UE_2}^{n_t} \cdots x_{i,UE_V}^{n_t}\right]$ is the coded signal vector. $\mathbf{z}^{n_r} \sim \mathcal{CN}(0, \sigma^2\mathbf{I})$ denotes the complex additive white Gaussian noise (AWGN) over the n_r-th BS receive antenna.

At the receiver MUD, the strongest UE is decoded first followed by SIC-based decoding to detect the rest of the UEs that are assumed to be arranged in descending order of their channel gains. Without loss of generality, let $w_{UE_v}^{n_r} \triangleq P_v^{UE}\left|h_{i,UE_v}^{n_t,n_r}\right|^2$ and $\lambda_{UE_v}^{n_r} \triangleq \frac{1}{\mathbb{E}(w_{UE_v}^{n_r})}$ denote the instantaneous received signal power and its mean value respectively. Prior to decoding, the receiver determines the instant decoding order π based on the instantaneous received UE signal power [32]. Subsequently, UEs are decoded in the sequence of $[UE_1, UE_2, \ldots, UE_V]$ with the instantaneous signal power relation $\left[w_{UE_1}^{n_r}, w_{UE_2}^{n_r}, \ldots, w_{UE_V}^{n_r}\right]$. The highest ranked UE experiences interference from all UEs while the lowest channel gain UE effectively enjoys interference-free transmission.

B. MULTI-ANTENNA SCMA SYSTEM

1) MIMO-SCMA TRANSMITTER

Uplink MIMO-SCMA systems utilize diversity and multiplexing based MIMO schemes and in particular, techniques associated with space diversity, Alamouti encoding and multiplexing [16]. In SCMA NOMA, each single antenna UE, assigned to a single codebook, utilizes $d_v < K$ REs while each RE can be accessed by $d_f < L$ UEs. In MIMO-SCMA, an uplink system in which one BS with N_r receive antennas and L UEs is considered where each UE is equipped with N_t antennas. Similar to the SCMA coder [21] for the n_t-th antenna, $n_t \in \{1, \ldots, N_t\}$. The coder operates L symbols $s^{n_t} = [s_1^{n_t}, s_2^{n_t}, \ldots, s_L^{n_t}] \in \mathbb{M}^{1\times L}$ in a cycle, where every $\log_2 M-$bit symbol for the l^{th} UE maps to one of the length $-K$ column vectors with $d_v, (d_v \leq K)$ used REs of sparse codeword matrix $C_l^{n_t} \in \mathbb{C}^{K\times M}$, resulting into complex codeword $x_l^{n_t} \in \mathbb{C}^{K\times 1}, l \in \{1, \ldots, L\}$. The combined codewords from all the L layers form the transmit vector on the n_t-th antenna, $\mathbf{x}_{n_t} \in \mathbb{C}^{K\times 1}$, transmitted over K REs. Three scenario outcomes are possible based on the UE-antenna multiplexing at the transmitter;

a: SPACE DIVERSITY

With space diversity SCMA (SD-SCMA), the codeword transmitted by each UE is repeated over the N_t transmit antennas for each UE. The signal received at the n_r-th antenna is given by

$$\mathbf{y}^{n_r} = \sum_{n_t=1}^{N_t}\sum_{l=1}^{L} diag(\mathbf{h}_l^{n_t,n_r})\mathbf{x}_l + \mathbf{z}^{n_r} \tag{2}$$

where $\mathbf{x}_l = [x_l^1, \ldots, x_l^K]$, $n_r \in \{1, \ldots, N_r\}$ and $\mathbf{h}_l^{n_t,n_r} = [h_1^{n_t,n_r,l}, \ldots, h_K^{n_t,n_r,l}]^T$ is the channel fading vector between the n_t transmit antenna of UE l and the n_r-th receive antenna, whose entries are supposedly independently and identically distributed (i.i.d) complex Gaussian random variable with zero mean and unit variance, while $\mathbf{z}^{n_r} \sim \mathcal{CN}(0, \sigma^2\mathbf{I})$ denotes the complex additive white Gaussian noise (AWGN) over the n_r-th receive antenna.

b: ORTHOGONAL SPACE TIME BLOCK CODING (OSTBC)

In Alamouti encoding, N_t data symbols are transmitted by N_t transmit antennas over T channel use periods. In particular, for the orthogonal space-time block code (OSTBC), $N_t = T = 2$ and can be characterized by the encoding matrix of $N_t \times T$. The signal received at the r^{th} antenna at the time slot $t \in \{t_0, t_{0+1}\}$ is given by

$$\mathbf{y}^{n_r} = \sum_{n_t=1}^{N_t}\sum_{l=1}^{L} diag(\mathbf{h}_l^{n_t,n_r})\mathbf{x}_l(n_t, t) + \mathbf{z}^{n_r} \tag{3}$$

where $\mathbf{x}_l(n_t, t)$ is the codeword sent by UE in layer l from the n_t-th antenna at time slot t.

c: SPATIAL MULTIPLEXING

For improved multiplexing gain, spatial multiplexing SCMA (SM-SCMA) is considered where the N_t transmit antennas at each UE are used for transmitting N_t independent SCMA codewords. At the n_r-th antenna, the received signal

$$\mathbf{y}^{n_r} = \sum_{n_t=1}^{N_t}\sum_{l=1}^{L} diag(\mathbf{h}_l^{n_t,n_r})\mathbf{x}_l(n_t) + \mathbf{z}^{n_r} \tag{4}$$

where $\mathbf{x}_l(n_t)$ is the distinct codeword sent by n_t-th antenna of UE in layer l.

Based on it's ability to transmit independent codewords at each transmit antenna, this work employs spatial multiplexing at the transmitter for multiplexing the power distinct UEs i.e., SUEs and MUEs superimposed at the same layer.

2) MIMO-SCMA RECEIVER

Taking advantage of the SCMA sparsity, the posterior probabilities at the receiver can be calculated through MPA [2] and log-MPA [33]. Denote by $I^{(\tau)}_{r_k\longrightarrow v_l}(\mathbf{x})$(respectively $I^{(\tau)}_{v_l\longrightarrow r_k}(\mathbf{x})$) the message corresponding to codeword $\mathbf{x}$ transmitted by (to) layer node (or rather, variable node, (VNs)) v_l to (by) receive node (resource node, (RNs)) r_k at the τ^{th} iteration. In each layer, the prior transmission probabilities of the codewords is uniform and given as $q^{n_t(\tau)}(\mathbf{x}) = \frac{1}{M}$. Based on the Bayesian [34], message between the VNs and RNs are updated as follows

$$I^{(\tau)}_{v_l\longrightarrow r_k}(\mathbf{x}_l) = \frac{q^{n_t(\tau)}(\mathbf{x}_l)}{I^{(\tau)}_{r_k\longrightarrow v_l}(\mathbf{x}_l)} \tag{5}$$

$$I^{(\tau)}_{r_k\longrightarrow v_l}(\mathbf{x}_l) = \frac{\Xi^{n_t(\tau)}_{r_k}(\mathbf{x}_l)}{I^{(\tau)}_{v_l\longrightarrow r_k}(\mathbf{x}_l)} \tag{6}$$

where

$$q^{n_t(\tau)}(\mathbf{x}_l) = I_{\Delta\to k}(\mathbf{x}_l^{n_t})\prod_{n_r}^{N_r}\prod_{k\in\mathcal{I}_v(l)} I^{(\tau-1)}_{r_k\longrightarrow v_l}\left(\mathbf{x}_{kl}^{n_t}\right) \tag{7}$$

$$\Xi^{n_t(\tau)}_{r_k}(\mathbf{x}_l) = I^{(\tau)}_{r_k\longrightarrow v_l}(\mathbf{x}_i)\sum_{\substack{\mathbf{x}_i\neq\mathbf{x}_k\\ i\in\mathcal{I}_r(k)}} P(y_n^{n_r}|\mathbf{x})\prod_{\substack{i\neq k\\ i\in\mathcal{I}_r(k)}} I^{(\tau)}_{v_i\longrightarrow r_k}(\mathbf{x}_i) \tag{8}$$

and $\mathcal{I}_v(l)$ and $\mathcal{I}_r(k)$ denote the set of resource node indices connected to variable node v_l, and the set of variable node indices connected to resource node r_k. The evaluation of (7) and (8) involve global searches over the joint space of all codewords of all layers, resulting in exponential computational complexity orders increasing the codebook size M and the degree of signal superposition d_f i.e., $\mathcal{O}(M^{d_f})$. As a result, MPA presents implementational challenges.

Compared to the MPA, EPA detection algorithm enjoys a salient advantage of linear complexity that scales M and d_f on a given RE, for SD-SCMA, OSTBC-SCMA and SM-SCMA schemes. EPA exhibits enhanced error rate performances due to the MIMO transmission. Additionally, EPA performance is dependent on the codebook size and the number of antennas. Consequently, EPA can be directly applied in the MUD for the three MIMO-SCMA schemes. In particular, it can be observed that an SM-SCMA scheme is equivalent to a SISO-SCMA system having N_tL users and an equivalent number of resources [16].

Expectation propagation regards the passing of messages between VNs and FNs as continuous random variables and thus approximates the real distribution as a Gaussian distribution, which can be expressed uniquely by the mean and variance. To this extent, the detection process can now be reduced to the computation of the mean and variance, which can avoid traversal of all codewords. Correspondingly, the equivalent probabilities for EPA at each RE can be expressed as

$$q^{n_t(\tau)}\left(x_{k,l}^{n_t}\right) \propto \mathcal{CN}\left(\mu_{kl}^{n_t(\tau)}, \sigma_{kl}^{n_t(\tau)}\right) \tag{9}$$

$$I_{v_l \longrightarrow r_k}^{n_t(\tau)} \propto \mathcal{CN}\left(\mu_{v_l \longrightarrow r_k}^{n_t(\tau)}, \sigma_{v_l \longrightarrow r_k}^{n_t(\tau)}\right) \tag{10}$$

$$I_{r_k \longrightarrow v_l}^{n_t(\tau)} \propto \mathcal{CN}\left(\mu_{r_k \longrightarrow v_l}^{n_t(\tau)}, \sigma_{r_k \longrightarrow v_l}^{n_t(\tau)}\right) \tag{11}$$

Using (9)-(11) in (5) and (6), the means and variances can be used to compute the messages. Based on [27], the EPA iterative process consists of the following steps;

1) Compute the posterior belief approximation $q^{n_t(\tau)}\left(\mathbf{x}_l^{n_t}|\mathbf{y}\right)$ as given in (7) for all $\mathbf{x}_l^{n_t} \in \mathcal{C}_l^{n_t}$ for each variable node $v_{l\in\mathcal{L}}$, where $\propto$ denotes equality up to scale and the uniform a-priori probability $I_{\Delta\to k}(\mathbf{x}_l^{n_t})$ given as,

$$I_{\Delta\to k}(\mathbf{x}_l^{n_t}) = \frac{1}{M}. \tag{12}$$

2) Compute the posterior mean $\mu_{kl}^{(\tau)}$ and variance $\sigma_{kl}^{(\tau)}$ for each variable node $v_{l\in\mathcal{L}}$ and resource node $r_{k\in\mathcal{I}_v(l)}$ as follows;

$$\begin{aligned}\mu_{kl}^{n_t(\tau)} &= \sum_{\mathbf{x}_l^{n_t}\in\mathcal{C}_l^{n_t}} q^{n_t(\tau)}\left(\mathbf{x}_l^{n_t}|\mathbf{y}\right)\cdot \mathbf{x}_{kl}^{n_t}\\ \sigma_{kl}^{n_t(\tau)} &= \sum_{\mathbf{x}_l^{n_t}\in\mathcal{C}_l^{n_t}} q^{n_t(\tau)}\left(\mathbf{x}_l^{n_t}|\mathbf{y}\right)\cdot \left|\mathbf{x}_{kl}^{n_t} - \mu_{kl}^{n_t(\tau)}\right|^2\end{aligned} \tag{13}$$

3) Evaluate the means $\mu_{v_l\longrightarrow r_k}^{n_t(\tau)}$ and the variances $\sigma_{v_l\longrightarrow r_k}^{n_t(\tau)}$ of the messages $I_{v_l\longrightarrow r_k}^{n_t(\tau)} \propto \mathcal{CN}\left(\mu_{v_l\longrightarrow r_k}^{n_t(\tau)}, \sigma_{v_l\longrightarrow r_k}^{n_t(\tau)}\right)$;

$$\begin{aligned}\sigma_{v_l\longrightarrow r_k}^{n_t(\tau)} &= \left(\frac{1}{\sigma_{kl}^{(\tau)}} - \frac{1}{\sigma_{r_k\longrightarrow v_l}^{n_t(\tau-1)}}\right)^{-1}\\ \mu_{v_l\longrightarrow r_k}^{n_t(\tau)} &= \left(\frac{\mu_{kl}^{n_t(\tau)}}{\sigma_{kl}^{n_t(\tau)}} - \frac{\mu_{r_k\longrightarrow v_l}^{n_t(\tau-1)}}{\sigma_{r_k\longrightarrow v_l}^{n_t(\tau-1)}}\right)^{-1}\end{aligned} \tag{14}$$

4) Determine the means $\mu_{r_k\longrightarrow v_l}^{n_t(\tau)}$ and the variances $\sigma_{r_k\longrightarrow v_l}^{n_t(\tau)}$ of the messages $I_{r_k\longrightarrow v_l}^{n_t(\tau)} \propto \mathcal{CN}\left(\mu_{r_k\longrightarrow v_l}^{n_t(\tau)}, \sigma_{r_k\longrightarrow v_l}^{n_t(\tau)}\right)$;

$$\begin{aligned}\mu_{r_k\longrightarrow v_l}^{n_t(\tau)} &= \frac{1}{h_l^{n_t,n_r}}\left(y_k^{n_r} - \sum_{\substack{i\in\mathcal{I}_r(k)\\ i\neq l}} h_l^{n_t,n_r}\cdot \mu_{v_i\longrightarrow r_k}^{n_t(\tau)}\right)\\ \sigma_{r_k\longrightarrow v_l}^{n_t(\tau)} &= \frac{1}{\left|h_l^{n_t,n_r}\right|^2}\left(N_0 - \sum_{\substack{i\in\mathcal{I}_r(k)\\ i\neq l}} \left|h_l^{n_t,n_r}\right|^2\cdot \sigma_{v_i\longrightarrow r_k}^{n_t(\tau)}\right)\end{aligned} \tag{15}$$

where $\mathcal{I}_r(k)$ denotes the set of variable node indices connected to resource node r_k.

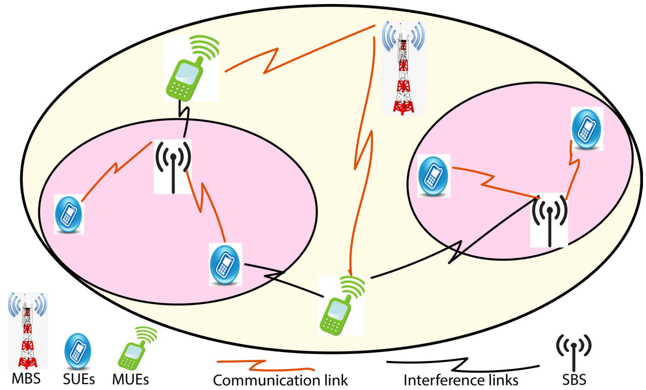

FIGURE 1. Uplink hybrid PD-SCMA HetNet model.

After τ_{max} iterations on (13), (14) and (15), $q^{n_t(\tau_{max})}\left(\mathbf{x}_l^{n_t}|\mathbf{y}\right)$ can be obtained and then the posterior LLRs $\Lambda_{kl}^{n_t}$ computed in a similar way as [27] given by (16). The iterations are initialized with $\mu_{r_k\longrightarrow v_l}^{n_t(0)} = 0$ and $\sigma_{r_k\longrightarrow v_l}^{n_t(0)} = \infty$ where ∞ is taken as a large positive constant.

$$\Lambda_{kl}^{n_t} = \log\frac{\sum_{\mathbf{x}_k\in\mathcal{X}_{k,l}^{+}} q^{n_t(\tau)}(\mathbf{x}_l)|\mathbf{y}}{\sum_{\mathbf{x}_k\in\mathcal{X}_{k,l}^{-}} q^{n_t(\tau)}(\mathbf{x}_l)|\mathbf{y}} \tag{16}$$

C. PD-SCMA SYSTEM

Consider a two-tier heterogeneous network (HetNet) model uplink PD-SCMA system of Fig. 1. The HetNet model comprises of a centralized macro base station (MBS) serving a set of $\mathcal{U}, (|\mathcal{U}| = U)$ randomly distributed macro cell users (MUEs) and underlaid set of $\mathcal{F}, (|\mathcal{F}| = F)$ small cells, each characterized by a centralized low power small cell base station (SBS) serving a set of $\mathcal{J}, (|\mathcal{J}| = J)$ uniformly distributed SUEs. A PD-SCMA transmitter operates L layers (of set $\mathcal{L}$), on which L independent symbol streams are transmitted. Employing RA schemes proposed in [8], encoded signals of single antenna V MUEs from the set $\mathcal{V}_{CB}, (|\mathcal{V}_{CB}| = V, \mathcal{V}_{CB} \in \mathcal{U})$ and one SUE ($J = 1$) form a layer L and are transmitted in the uplink to single antenna BSs. The MUEs and SUEs are co-multiplexed on the set of available codebooks (CB) from set $\mathcal{CB} = \{1, \cdots CB\}$ designed from complex mapping of the time-frequency $\mathcal{K} = \{1, \cdots K\}$ REs. The $K-$dimensional codewords of a codebook are sparse vectors with d_v ($d_v < K$) nonzero entries corresponding to d_v specific REs for a user.

A PD-SCMA system employs V-BLAST encoding to obtain branch multiplexed signals, forward error correction (FEC) for correcting random error by introducing redundancy and interleaving to resist consecutive errors through scattering the data stream. Every $\log_2 M$-bit symbols are encoded to a length $-K$ sparse vector resulting into complex codewords $\mathbf{s}^{SUE_j} = \left[s^{SUE_{j,1}}, \ldots, s^{SUE_{j,K}}\right]^T$ and $\mathbf{s}^{MUE_v} = \left[s^{MUE_{v,1}}, \ldots, s^{MUE_{v,K}}\right]^T$ for SUEs and MUEs respectively. The vectors $\mathbf{s}^{SUE_j}$ and $\mathbf{s}^{MUE_v}$ belongs to a finite set of $\mathbb{M}, |\mathbb{M}| = M$ codewords of codebook $\mathcal{CB}$. Each codebook can be utilized by one user, like for conventional SCMA or several users superimposed in the codebook, as with PD-SCMA system by allocating users with distinct power levels.

We adopt the codebook assignment, user pairing and power allocation proposed in [8]. Assuming synchronized transmission, the received vector can be given by

$$\mathbf{y} = \sum_{l=1}^{L} diag(\mathbf{h}_l)\mathbf{x}_l + \mathbf{z} \tag{17}$$

where $\mathbf{h}_l = [h_l^{SUE_j} h_l^{MUE_1} \cdots h_l^{MUE_V}]$. The channel vectors $h_l^{SUE_j} = [h_{l,1}^{SUE_j}, \ldots, h_{l,K}^{SUE_j}]^T$ and $h_l^{MUE_v} = [h_{l,1}^{MUE_v}, \ldots, h_{l,K}^{MUE_v}]^T$. The codeword vector $\mathbf{x}_l$ is drawn from the the SUE and MUE codebooks multiplexed in layer l given by $\mathbf{x}_l = \left[\mathbf{x}_l^{SUE_j} \mathbf{x}_l^{MUE_1} \cdots \mathbf{x}_l^{MUE_V}\right]$. The entries $\mathbf{x}_l^{SUE_j} = \sqrt{P_l^{SUE_j}} \cdot \mathbf{s}^{SUE_j}$ and $\mathbf{x}_l^{MUE_v} = \sqrt{P_l^{MUE_v}} \cdot \mathbf{s}^{MUE_v}$ and $P_l^{SUE_j}$ and $P_l^{MUE_v}$ are the normalized SUE and MUE power levels respectively.

At the receiver, authors in [7] and [8] propose a joint MUD that iteratively decodes the received messages using log-MPA in the code-domain and SIC in the power-domain. The performance of the joint MUD is tied to the system's point of operation being within the multiplexing bounds.

III. PROPOSED MIMO BASED PD-SCMA

A SM multi-antenna based PD-SCMA transmitter (M-PD-SCMA) on a two-tier HetNet model of Fig. 1 is considered. Each user and BS has N_t and N_r transmit and receive antennas respectively. The M-PD-SCMA transmitter consists of three stages; Firstly, the resource allocation (RA) stage, where the REs, codebooks and power are assigned to user symbols and individual users respectively.User pairing and clustering procedures are then deployed. Secondly, layered power domain (PD) multiplexing stage where codeword selection and multiplexing of the selected codewords from clustered users in PD is done. Lastly, antenna assignment stage where summed codewords from each layer are allocated to an antenna.

Similarly, to recover the approximate transmitted user symbol $\hat{\mathbf{s}}$, the MUD operates the received signal at n_r in two stages; Firstly, modified EPA iterative process where iterative detection of the codewords is executed, followed by user symbols reconstruction realized by computing the posterior log likelihood ratios (LLRs). Secondly, SIC process where the signals of users with weaker channel conditions are decoded and subtracted from the received codeword.

A. MIMO-BASED PD-SCMA TRANSMITTER

The block diagram of the uplink M-PD-SCMA transmitter for n_t-th antenna is shown in Fig. 2. Users are paired to form L clusters, where each cluster is assigned a unique codebook utilizing distinct REs. Similar to the conventional SCMA, a PD-SCMA transmitter operates L layers (of set $\mathcal{L}$), on which L independent symbol streams are transmitted. A layer is constructed by drawing select codewords from each user in the cluster matched to the layer i.e., $J = 1$ SUE and V MUEs from the set $\mathcal{V}_{CB}$, ($|\mathcal{V}_{CB}| = V$, $\mathcal{V}_{CB} \in \mathcal{U}$). This implies that each layer constitutes of $M = (V + 1)$ users' codewords and SUE to layer is a one-to-one matching, $L = J$. Prior to transmission, the M-PD-SCMA performs the following steps;

1) *Resource Allocation:* Followed by V-BLAST encoding, forward error correction (FEC) and interleaving, every $log_2(M)$-bit user symbols are mapped, according to SCMA encoding, to a length$-K$ sparse vector resulting into complex codewords $\mathbf{s}^{SUE_{j,n_t}}$ and $\mathbf{s}^{MUE_{j,n_t}}$ respectively given by

$$\begin{aligned}\mathbf{s}^{SUE_{j,n_t}} &= \left[s^{SUE_{j,1,n_t}}, \ldots, s^{SUE_{j,K,n_t}}\right]^T,\\ \mathbf{s}^{MUE_{j,n_t}} &= \left[s^{MUE_{v,1,n_t}}, \ldots, s^{MUE_{v,K,n_t}}\right]^T\end{aligned} \tag{18}$$

These vectors belong to a finite set of $\mathcal{M}$, ($|\mathcal{M}| = M$) codewords of a codebook CB. As an example from Fig. 2, each CB comprises of $M = 4$ codewords, $\mathcal{M} = \{0, 1, 2, 3\}$. The entries $\mathbf{s}^{SUE_{j,n_t}}$ and $\mathbf{s}^{MUE_{v,n_t}}$ denote respectively the j^{th} SUE and v^{th} MUE mapped to the k^{th} RE on a CB for the n_t-th antenna. The user information symbols utilize RE_1 and RE_2 of codebook CB_1. Subsequently, the transmitter performs codebook and power allocation utilizing RA schemes proposed in [8]. After RA, MUEs are paired with a SUE on a codebook using a user pairing scheme to form the L clusters.

2) *Layered PD Multiplexing:* For the transmitting antenna n_t, a codeword from each pairing user in the cluster is selected. The selected codewords are consolidated resulting into a layer $\mathbf{X}_l^{n_t}$ given as

$$\mathbf{X}_l^{n_t} = \left[\mathbf{x}_l^{SUE_{j,n_t}} \mathbf{x}_l^{MUE_{1,n_t}} \cdots \mathbf{x}_l^{MUE_{V,n_t}},\right] \in \mathbb{C}^{K\times M} \tag{19}$$

The entries $\mathbf{x}_l^{SUE_{j,n_t}} = \sqrt{P_l^{SUE_j}} \cdot \mathbf{s}^{SUE_{j,n_t}}$ and $\mathbf{x}_l^{MUE_{v,n_t}} = \sqrt{P_l^{MUE_v}} \cdot \mathbf{s}^{MUE_{v,n_t}}$ and $P_l^{SUE_j}$ and $P_l^{MUE_v}$ are the normalized SUE and MUE power levels respectively. The codewords in $\mathbf{X}_l^{n_t}$ are then multiplexed in power domain by diversifying the allocated power levels of the users in the clusters resulting to the layer message vector $\mathbf{x}_l^{n_t} \in \mathcal{C}^{K\times 1}$.

3) *Antenna Assignment:* The vectors $\mathbf{x}_l^{n_t}$ from all the L layers are then summed together to obtain the transmit vector $\mathbf{x}^{n_t} \in \mathcal{C}^{K\times 1}$. The transmit message vector $\mathbf{x}^{n_t}$ is assigned to the n_t-th antenna and transmitted over the K subcarriers. Note that in the subsequent antenna n_{t+1}, the transmitter selects and transmits different codewords from the users in a cluster. The transmitter algorithm is presented in Algorithm 1.

Under the constraint that no two layers should be assigned all the same REs for an affordable complexity order, the system loading is given as $\lambda = M \times \binom{L}{d_v}$. The transmitted codeword signals from all layers go through a Rayleigh flat-fading channel. The received signal vector after at the $n_r - th$

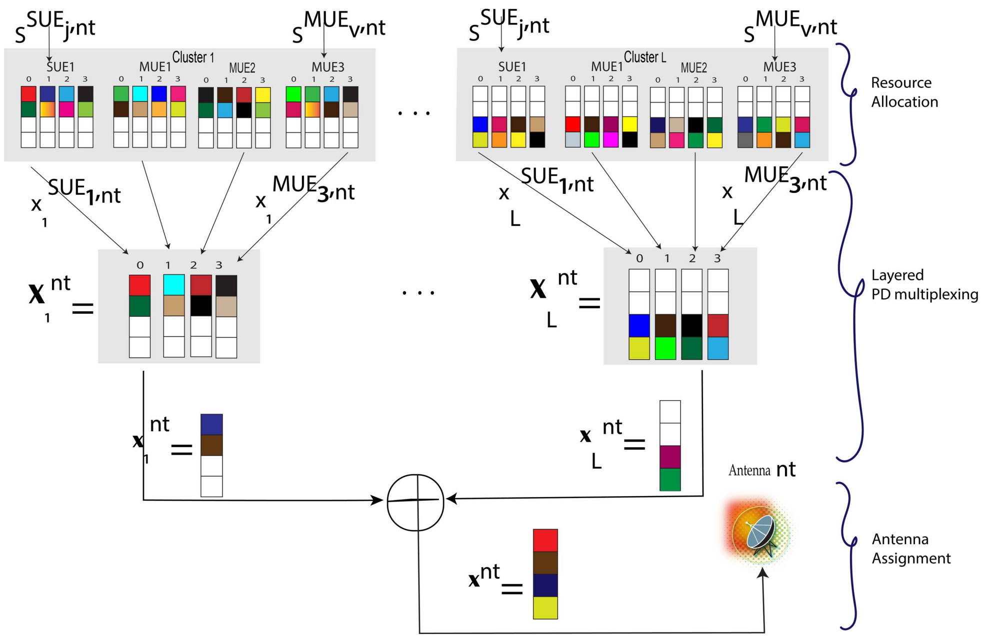

FIGURE 2. System model of the proposed uplink spatial multiplexing-based M-PD-SCMA system with $M = 4$ codewords.

Algorithm 1 M-PD-SCMA Transmitter Algorithm

Initialization Initialize the sets: $\mathcal{F}, \mathcal{U}, \mathcal{V}, \mathcal{J}$ and $\mathcal{L}$.
Stage I: Resource allocation
  Sparse encoding of incoming user symbols, eqn. (1).
for MUEs $v = 1 : V$ **do**
  MUE power allocation, $P_l^{MUE_v}$.
end for
for SBS $f = 1 : F$ **do**
  for SUE $j = 1 : J$ and $l = 1 : L$ **do**
    SUE power allocation, $P_l^{SUE_j}$.
    Codebook assignment to SUEs.
  end for
  SUE-MUEs pairing and clustering.
Stage II: Layered PD multiplexing
  for SUE $n_t = 1 : N_t$ and $m = 1 : M$ **do**
    Select codeword m from each user in cluster l and integrate them to obtain $\mathbf{X}_l^{n_t}$, eqn. (19).
    Perform PD multiplexing of message vectors in $\mathbf{X}_l^{n_t}$ to obtain $\mathbf{x}_l^{n_t}$.
Stage III: Antenna assignment
    Sum the codewords $\mathbf{x}_l^{n_t}$ from all the L layers to obtain $\mathbf{x}^{n_t}$.
    Perform layer - antenna assignment.
    Transmit $\mathbf{x}^{n_t}$ through antenna n_t.
  end for
end for

receiving, $\mathbf{y}^{n_r}$ reads,

$$\mathbf{y}^{n_r} = \sum_{n_t=1}^{N_t} \sum_{l=1}^{L} diag(\mathbf{h}_l^{n_t,n_r})\mathbf{x}_l^{n_t} + \mathbf{z}^{n_r} \tag{20}$$

where $\mathbf{h}_l^{n_t,n_r} = [h_{l,SUE_j}^{n_t,n_r} h_{l,MUE_1}^{n_t,n_r} \cdots h_{l,MUE_V}^{n_t,n_r}]$. Through the $n_r - th$ receive antenna, $h_{l,SUE_j}^{n_t,n_r}$ and $h_{l,MUE_v}^{n_t,n_r}$ denote SUE and MUE channel coefficients averaged over the d_v in each layer l respectively. The overall MIMO channel matrix associated with the $l-$th layer can be represented $\mathbf{H}_l \in \mathbb{C}^{N_r \times V}$. Obtaining the precise channel state information (CSI) for signal detection may not be achievable in practice as a result of imperfect channel estimation. Taking into account the channel estimation error, the noisy channel estimation is modeled as

$$\mathbf{H}_l = \hat{\mathbf{H}}_l + e\Gamma_l \tag{21}$$

where $e\Gamma_l$ is the channel estimation error, which is uncorrelated with $\mathbf{H}_l$. Γ_l follows an i.i.d. complex Gaussian distribution with zero mean and unit variance; e is the accuracy of channel estimation [35].

In the uplink, since the PD-SCMA codewords from different clusters are not multiplied by the same fading channel, a modified EPA MUD based should be considered. Consequently, we employ a normalized channel coefficient $g_l^{n_t,n_r}$ of the multiplexed layer signal given by

$$g_l^{n_t,n_r} = \sqrt{\left(|h_{l,SUE_j}^{n_t,n_r}|^2 + \sum_{v=1, v\in\mathcal{V}_{CB}}^{V} |h_{l,MUE_v}^{n_t,n_r}|^2\right)} \tag{22}$$

This is then used in the presented modified EPA algorithm.

B. MIMO-BASED PD-SCMA RECEIVER

A low complex modified joint EPA-SIC receiver is proposed for the uplink system. Different from the joint MUD for

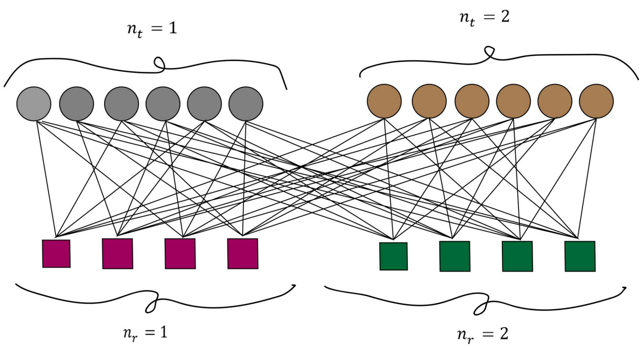

FIGURE 3. Extended factor graph representation for a SM based M-PD-SCMA with $L = 6$ and $K = 4$ for $n_t = 2$ and $n_r = 2$.

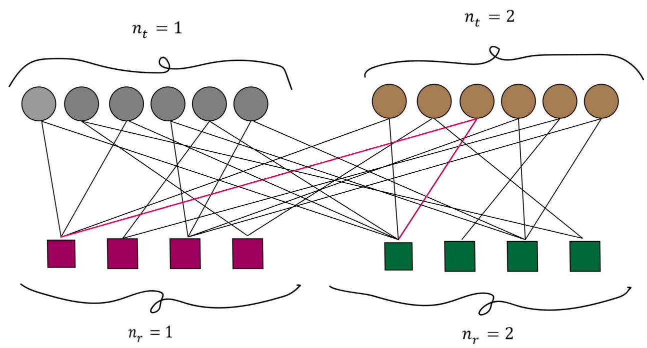

FIGURE 4. Extended factor graph after QR decomposition. The number of edges are reduced and the factor graph is less dense.

PD-SCMA in [8], the M-PD-SCMA MUD performs two steps iteratively at antenna n_r for all the layers i.e., modified EPA process in the SCMA dimension and SIC process in the PD-NOMA dimension. The details of the the individual MUDs process are discussed as follows;

1) MODIFIED EPA PROCESS

Unlike in MPA [20], EPA only pursues the means and variances of the transmitted messages during the iterative detection on the factor graph. An extended factor graph representation for $n_t = n_r = 2$ is illustrated in Fig. 3. The circles and squares represent the layer node (variable node, (VNs)) and receive node (resource node, (RNs)) respectively. Here, the factor graph is comprised of LN_t variable nodes v_l and KN_r resource nodes r_k, for which each variable node is a PD multiplexed symbol of M users. The complexity of the EPA greatly depends on the number of messages passing. Since the transmitted codewords are sparse, the number of messages passing in Fig. 3 is proportional to N_rKd_f. However, with increasing codebook size M and receiving antennas N_r, the complexity is still substantial owing to the extended graph density with a sizeable number of edges. As a result, the performance of the EPA is limited to some extent especially for larger codebooks and massive MIMO applications.

In order to achieve lower complexity and improved decoding convergence, we employ a modified near-optimal EPA based on channel matrix sparsity (SC-EPA) proposed in [29]. SC-EPA aims at making the extended factor graph less dense by applying the QR decomposition to $\mathbf{H}$. Basically, the SC-EPA improves upon the EPA by considering the sparsity of the channel matrix. For the entries that change to zero, it is considered that there is no message passing between two corresponding points in the extended factor graph. Subsequently, the number of active edges is significantly reduced.

The effect of the channel matrix sparsing through QR decomposition can be illustrated in Fig. 4. Intuitively, the number of messages passing and edges greatly reduces therefore reducing the complexity without performance penalties. Denote by ζ, the ratio of nonzero entries in the equivalent QR decomposed matrix (denoted by $\mathbf{H}_k$) compared with $\mathbf{H}_k$. Since the ratio of the non-zero entries for all K REs, ζ can represent the reduction of message passing in the extended factor graph and is given as $\zeta = \frac{d_f + 1}{2N_r}$. Besides, the number of messages passed after QR decomposition is autonomic of the number of receiving antennas, N_r, as shown in Fig. 4.

In order to improve the EPA, new message passing between VNs and FNs have been proposed. For the VN to FN message passing in EPA (15), $\sigma^{n_t(\tau)}_{v_l \longrightarrow r_k}$ constitutes many reciprocal operations while the computation of $\mu^{n_t(\tau)}_{v_l \longrightarrow r_k}$ relies on the values of $\sigma^{n_t(\tau)}_{v_l \longrightarrow r_k}$. This feature strains the EPA process by hindering the algorithm computational uniformity. Accordingly, a factor α is introduced as in (23)

$$\alpha = \frac{\sigma^{n_t(\tau)}_{r_k \longrightarrow v_l}}{\sigma^{n_t(\tau)}_{r_k \longrightarrow v_l} - \sigma^{n_t(\tau)}_{kl}} \tag{23}$$

The computation of $\sigma^{n_t(\tau)}_{v_l \longrightarrow r_k}$ and $\mu^{n_t(\tau)}_{v_l \longrightarrow r_k}$ in (15) then simplifies to (24) and (25) respectively. In this way, the number of inverse operations is reduced to one and the algorithm computation uniformity is significantly improved.

$$sigma^{n_t(\tau)}_{v_l \longrightarrow r_k} = \alpha \sigma^{n_t(\tau)}_{kl} \tag{24}$$

$$\mu^{n_t(\tau)}_{v_l \longrightarrow r_k} = \mu^{n_t(\tau)}_{kl} + \alpha\left(\mu^{n_t(\tau)}_{kl} - \mu^{n_t(\tau-1)}_{r_k \longrightarrow v_l}\right) \tag{25}$$

To further minimize waste of many computational resources, message passing from FNs to VNs can be improved. The algorithm first computes the estimated received signal $\hat{\mathbf{y}}^{n_r}$ (20). Then the estimates of the mean $\hat{\mu}^{n_t(\tau)}_{kl}$ and variance $\hat{\sigma}^{n_t(\tau)}_{kl}$ evaluated as below,

$$\hat{\mu}^{n_t(\tau)}_{kl} = \sum_{k \in F(n)} g^{n_t,n_r}_{l,n} \mu^{n_t(\tau-1)}_{v_l \longrightarrow r_k} \tag{26}$$

$$\hat{\sigma}^{n_t(\tau)}_{kl} = \sum_{k \in F(n)} |g^{n_t,n_r}_{l,n}|^2 \sigma^{n_t(\tau-1)}_{v_l \longrightarrow r_k} + \sigma^2_z \tag{27}$$

Substituting (26) - (27) into (15), we obtain,

$$\mu^{n_t(\tau)}_{r_k \longrightarrow v_l} = \frac{1}{g^{n_t,n_r}_l}\left(\mathbf{y}^{n_r}_k - \hat{\mu}^{n_t(\tau)}_{kl}\right) + \mu^{n_t(\tau-1)}_{v_l \longrightarrow r_k} \tag{28}$$

$$\sigma^{n_t(\tau)}_{r_k \longrightarrow v_l} = \frac{\hat{\sigma}^{n_t(\tau)}_{kl}}{|g^{n_t,n_r}_l|^2} - \sigma^{n_t(\tau-1)}_{v_l \longrightarrow r_k} \tag{29}$$

2) SUCCESSIVE INTERFERENCE CANCELLATION PROCESS

Having successfully recovered a layer, SIC is employed to detect the M PD multiplexed users. Prior to decoding, the receiver computes the decoding order metric $\mathcal{N}_l$ proposed in [8] for layer l. Then, the instant decoding order π is determined based on the instantaneous received user signal power. Subsequently, users are decoded in the sequence $\left[MUE_1, MUE_2, \ldots, MUE_V, SUE_j\right]$. The highest ranked user experiences interference from all users while the lowest channel gain user effectively enjoys interference-free transmission.

The instantaneous received SINR at n_r of the v^{th} MUE multiplexed at layer l, $\gamma_{v,l}^{MUE,n_r}$ is given by

$$\gamma_{v,l}^{MUE,n_r} = \frac{w_{MUE_{v,l}}^{n_r}}{\sum\limits_{i=v+1}^{V} w_{MUE_{v,l}}^{n_r} + \phi_l}, \tag{30}$$

while that of the V^{th} MUE is given by

$$\gamma_{V,l}^{MUE,n_r} = \frac{w_{MUE_{V,l}}^{n_r}}{\phi_l}, \tag{31}$$

The SINR at n_r of the j^{th} SUE, $\gamma_{j,l}^{SUE,n_r}$, after successful SIC of all MUEs $v \in \mathcal{V}_{CB}$ in each layer is given by

$$\gamma_{j,l}^{SUE,n_r} = \frac{P_l^{SUE_j}\left|h_{l,SUE_j}^{n_t,n_r}\right|^2}{\sigma_{j,l}^2}. \tag{32}$$

The achievable data rate, $R_{j,l}^{SUE,n_r}$ is given as

$$R_{j,l}^{SUE,n_r} = \log_2\left(1 + \gamma_{j,l}^{SUE,n_r}\right), \tag{33}$$

while that of the MUEs is similarly derived and given as

$$R_{v,l}^{MUE,n_r} = \log_2\left(1 + \gamma_{v,l}^{MUE,n_r}\right), \tag{34}$$

Lastly, after SIC decoding on each layer, the symbol estimates for each user over the layer can be obtained by log-like ratio (LLR) computation via (16). The M-PD-SCMA joint modified EPA-SIC receiver algorithm is given in Algorithm 2.

Algorithm 2 M-PD-SCMA Joint Modified EPA-SIC Receiver Algorithm

Input variables: $LN_t \times KN_r \times M$ channel matrix $\mathbf{H}$, Layers $\mathcal{L}$, $N_r \times 1$ noise vector.
Output variables: the posterior LLRs $\Lambda_{kl}^{n_t}$ in (16)
Initialization: $\mu_{v_l \longrightarrow r_k}^{n_t(0)} = 0$, $\sigma_{v_l \longrightarrow r_k}^{n_t(0)} = \infty$ and $I_{\Delta \to k}(\mathbf{x}_l^{n_t}) = \frac{1}{M}$.
for SBS $f = 1 : F$ **do**
  for $n_r = 1 : N_r$ and $l = 1 : L$ **do**
    Compute the $KN_r \times 1 \times M$ received signal vector $\mathbf{y}$.
    Step I. EPA process and symbol reconstruction
    for Iteration $\tau = 1 : \tau_{Max}$ **do**
      Compute $q^{n_t(\tau)}\left(\mathbf{x}_l^{n_t}|\mathbf{y}\right)$, eqn. (7).
      Compute $\mu_{kl}^{n_t(\tau)}$ and $\sigma_{kl}^{n_t(\tau)}$, via (13).
      Compute $\sigma_{v_l \longrightarrow r_k}^{n_t(\tau)}$, via (24) and $\mu_{v_l \longrightarrow r_k}^{n_t(\tau)}$, via (25).
      Compute $\hat{\mu}_{kl}^{n_t(\tau)}$, via (26) and $\hat{\sigma}_{kl}^{n_t(\tau)}$, via (27).
      Compute $\mu_{r_k \longrightarrow v_l}^{n_t(\tau)}$, via (28) and $\sigma_{r_k \longrightarrow v_l}^{n_t(\tau)}$, via (29).
    end for
    Step II. SIC process
    Compute the decoding order metric $\mathcal{N}(l)$.
    Determine the resultant decoding order π.
    Perform SIC on the user with highest received power.
    $\mathcal{N}(l) = \mathcal{N}(l) - 1$.
    Compute and compare symbol-wise LLRs via (16).
  end for
end for

C. COMPLEXITY ANALYSIS

The complexity of the EPA primarily relies on the messages passing between the VNs and the FNs. Setting the FNs as the starting point in the computational process, the messages are first updated froms FNs to VNs exhibiting a complexity $\mathcal{O}\left(KN_r d_f(2d_f + 3M) + 3Kd_f M\right)$. Secondly, the messages passing from VNs to FNs are updated exhibiting a complexity $\mathcal{O}\left(3KN_r d_f\right)$. Lastly, the posterior likelihood ratio are calculated after algorithm convergence. It can be observed that the complexity of EPA linearly scales both M and the degree of superposition d_f on a given RE which is lower than the message passing algorithm (MPA) counterpart exhibiting $\mathcal{O}\left(KN_r M^{N_t d_f}\right)$.

Compared with the conventional EPA, the proposed modified EPA greatly reduces the number of messages passing by employing the QR decomposition. Additionally, the proposed way of message passing from the VNs to FNs not only reduces the complexity but also increases the parallelism of the algorithm. The complexity in message passing from FNs to VNs reduces to $\mathcal{O}\left(KN_r d_f M\right)$ while message passing from VNs to FNs reduces to $\mathcal{O}\left(KN_r d_f\right)$.

The complexity of SIC is primarily in the computation of the decoding order metric for each user multiplexed in the layer, and is given as $\mathcal{O}(b^3)$ for a MMSE transformation weight matrix of $b \times b$. Consequently, the overall J-EPA-SIC receiver complexity can approximately be given by $\mathcal{O}\left(N_t KN_r Md_f + Mb^3\right)$.

IV. OUTAGE PROBABILITY ANALYSIS

The layer outage probability of the fading imperfect channels based on the time-varying received power strength for each user superimposed in the layer is analysed. The PD multiplexed users (SUE and MUEs) consolidated into a layer such that the diversity in the power levels is maximized for optimized SIC at each antenna. With deteriorating and imperfect channel conditions and SIC constraints, transmission reliability is not guaranteed. From (20) and (22), the desired layer component is weighted with the sum of the squared absolute values of the channel coefficients of the $M = V + 1$ multiplexed users in a layer and given as $r_l = \left(g_l^{n_t,n_r}\right)^2$. Subsequently, the SINR of the m^{th} MUE at layer l can then be written as

$$\gamma_l = \frac{d_v r_l P_{l,c}^{MUE}}{\sum_{i=1}^{M} K r_l P_{i,c}^{MUE} + z_l} \tag{35}$$

A channel outage is said to occur when the SINR γ_l falls below the required threshold γ_l^{rq} [36].

Since the MUEs in the macro cell access the common MBS resource transmit power, a user-wise decoupled mapping of channel coefficients to SINR becomes impossible. It is therefore imperative to define the channel outage probability of the system directly on the variables r_l as;

$$\pi_{out} = \int_{\mathcal{H}} \left(\prod_{l=1}^{L} f_{r_l}(r_l) dr_l \right) \tag{36}$$

where $\mathcal{H}$ denotes all the infeasible channels i.e., the set of channels in which the SINR requirements $\gamma_1^{rq}, \ldots, \gamma_L^{rq}$ cannot be fulfilled with non-negative powers $P_l > 0, \sum_{l=1}^{L} P_l < P_{max}$. In this way, at least one user, will exhibit an outage.

In this multi-user scenario where users jointly access transmit powers, the outage events of the different layers experience mutual dependencies. An acceptable approach is the formulation for the set of channel outage events $\mathcal{H}$. Using (35), the implicit description for the set $\mathcal{H}$ of the infeasible channel realizations can be obtained as

$$\mathcal{H} = \{r_1, \ldots, r_L | r_L < r_L^{th}\}, \tag{37}$$

where

$$r_L^{th} = \lim_{\epsilon \longrightarrow 0^+} \frac{r_L^{rq} \sigma_l^2}{max\{(d_v - r_L^{rq} K) P_{max} - d_v \sum_{i=1}^{L-1} P_i, \epsilon\}} \tag{38}$$

The expression for r_L^{th} can be obtained from (35) when computing the power available in layer l by subtracting necessary powers for all other users from P_{max}. If the channels $r_1, \ldots, r_{L-1}$ already cause an outage by requiring more power than P_{max}, then

$$P_l = P_{max} - \sum_{i=1}^{L-1} P_i < \frac{\gamma_l^{rq}}{d_v} \left(K P_{max} + \frac{\sigma_l^2}{r_l} \right) \tag{39}$$

Using $\lim_{\epsilon \longrightarrow 0^+} \frac{1}{\epsilon} = \infty$, (37) and (38) transforms to the trivial condition $r_L < \infty$. With the definition of $\mathcal{H}$ in (37), the L^{th} order integral defined (36) can then be computed as

$$\pi_{out} = \int_0^{\infty} \cdots \int_0^{r_L^{th}} \int_0^{(r_1, \ldots, r_{L-1})} \prod_{l=1}^{L} f_{r_l}(r_l) dr_l. \tag{40}$$

After some mathematical manipulations, the analytical lower and upper bound can be computed by first defining strict subsets $\mathcal{H}^{lb}$ and $\mathcal{H}^{lb}$ respectively given as

$$\begin{aligned} \mathcal{H}^{lb} &= \{r_1, \ldots, r_L | \exists\, r_k < r_k^{(lb)}\} \\ \mathcal{H}^{up} &= \{r_1, \ldots, r_L | \exists\, r_k < r_k^{(up)}\} \end{aligned} \tag{41}$$

with

$$r_k^{(lb)} = \frac{\gamma_l^{rq} \sigma_l^2}{\left(d_v - \gamma_l^{rq} K \right) P_{max}}$$

$$r_k^{(up)} = \begin{cases} \dfrac{\gamma_l^{rq} \sigma_l^2}{\left(d_v - \sum_{l=1}^{L} \gamma_l^{rq} K \right) P_{max} - \sum_{i=1}^{L-1} \frac{\sigma_0^2}{r_i^{(up)}}}, & \text{for} l = L \\ \dfrac{r_i^{(lb)}}{r_K^{(lb)}} r_K^{(up)}, & l \neq L \end{cases} \tag{42}$$

From (41), (42) and following the work of [36], the resultant lower and upper bounds can be given respectively as below,

$$\begin{aligned} \pi_{out}^{lb} &= \int_{\mathcal{H}^{lb}} \left(\prod_{l \in L} f_{r_l}(r_l) \right) dr_l, \quad \pi_{out}^{lb} < \pi_{out} \\ \pi_{out}^{up} &= \int_{\mathcal{H}^{up}} \left(\prod_{l \in L} f_{r_l}(r_l) \right) dr_l, \quad \pi_{out}^{up} > \pi_{out}. \end{aligned} \tag{43}$$

V. RESULTS AND DISCUSSION

The analytical evaluation of the M-PD-SCMA is presented. Firstly, we present the bit error rate (BER) comparison at different receive antennas. Secondly, the system capacity is analysed in a similar way to [8], considering performance with varying number of layers, SNR and the effect of the channel error. Thirdly, the outage performance is analysed with respect to the number of layers and the maximum power to layer power ratio. It is assumed that the SUE multiplexed in layer with MUEs are low powered and that all MUEs draw their power from the MBS subject to $\sum_{l=1}^{L} \sum_{v \in \mathcal{V}_{CB} \in \mathcal{U}} P_l^{MUE_v} = P_{max}$. Lastly, the convergence rate and complexity performance of the uplink M-PD-SCMA system are presented.

TABLE 2. Simulation parameters.

Parameters	Values
Center carrier frequency	$2\,GHz$
MBS coverage radius	$500\,m$
SBS coverage radius	$50\,m$
Maximum transmission power	$23\,dBm$
Noise variance, σ_x^2	$-174\,dBm$
Distance path loss	$PL(dB) = 128.1 + 37.6 \log_{10} D$
Fast fading channel model	$g_{f,k,c}^{SUE}, g_{m,c}^{MUE} \sim \mathcal{CN}(0, 1)$
RU Bandwidth	$200\,kHz$
Minimum transmission rate	$5\,Mbps/Hz$
Interference threshold	$10^{-5.5}\,W$

Denote by ρ the maximum number of bits per user transmitted by two antennas during two transmission channel slots. We consider a SM based M-PD-SCMA that transmits 4 codewords which is equivalent to $\rho = 8$ bits/user/2 transmit antennas/2 channel use periods, when a codebook of size $M = 4$ codewords is employed. The detailed system parameters and assumptions are presented in Table 2.

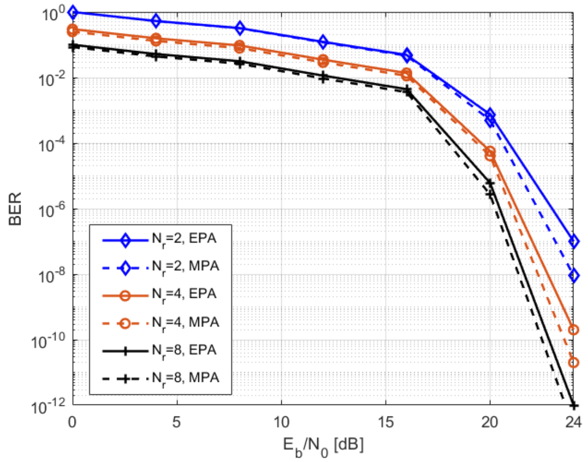

FIGURE 5. BER performance versus N_r with $\rho = 4$.

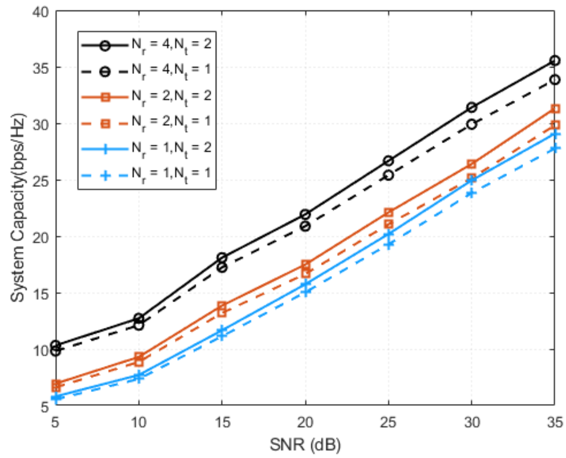

FIGURE 7. Capacity versus SNR.

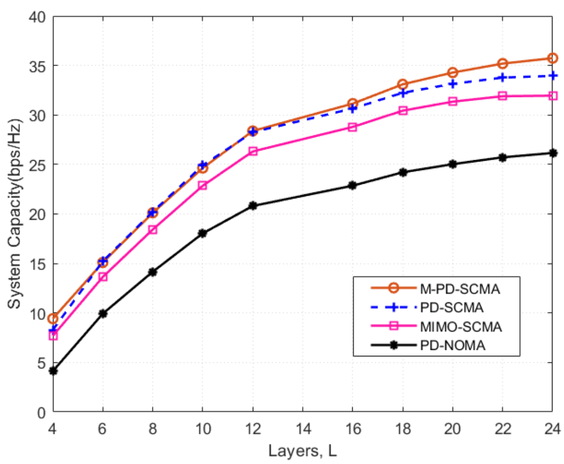

FIGURE 6. Capacity vs number of SUEs.

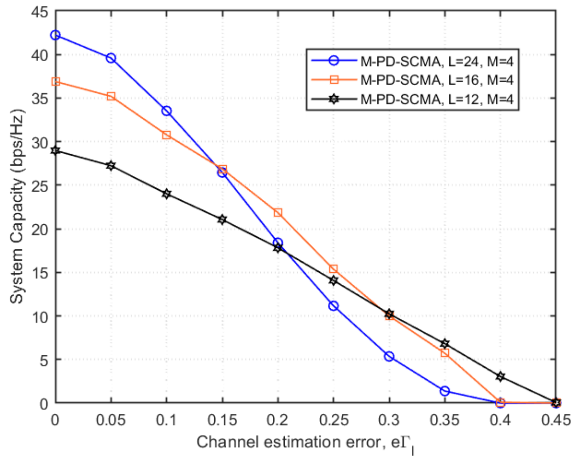

FIGURE 8. System capacity vs channel estimation error.

Similar to numerical analysis done in [20], Fig. 5 represents the BER performance as the number of antennas grows for both MPA- and EPA- based M-PD-SCMA schemes. For both receiver schemes, the BER performance improves as the number of receive antennas increases. The EPA based receiver closely approximates the near-optimal MPA based receiver even for higher number of antennas. Therefore, by employing more antennas, the EPA detector can achieve a near optimal performance with low complexity. Comparatively, BER in the downlink system [20] outperforms the uplink system under the same performance metrics. Unlike in the downlink, uplink UEs superimposed in a layer experience different channel conditions characterised by temporal correlation of the fading coefficients at each RE at different times. This affects the BER performance at varying number of antennas.

Fig. 6 depicts the system capacity versus the number of SUEs/layers in comparison with other NOMA schemes. It can be observed that the system capacity for all schemes increase sharply for low number of SUEs up to approximately 12 SUEs (12 layers), beyond which the capacity growth is gradual. Increasing the number of layers results in aggravated interference that degrades the performance. This implies that the optimal capacity can be obtained when the number of users is within the multiplexing bounds. It can be observed that M-PD-SCMA capacity benchmarks PD-SCMA and evidently outperforms MIMO-SCMA and the PD-NOMA scheme. This can be attributed to the multiplexing and diversity gains of MIMO achieved by using SM. Besides, the efficient spectral RE utilization associated with the RA schemes ascribes to superior system capacity in both M-PD-SCMA and PD-SCMA.

Fig. 7 illustrates the system capacity versus signal to noise ratio (SNR) for different number of transmit and receive antennas. Using 12 layers and $\rho = 4$, capacity increases monotonically with the SNR for different values of N_r. In fact, it can be observed that employing higher number of antennas achieves a higher capacity due to enhanced spatial multiplexing order. In varying the N_t, the capacity closely follows the capacity for different values of N_r hence satisfactorily justifying the use of lowered number of transmit antennas for the same achieved system capacity.

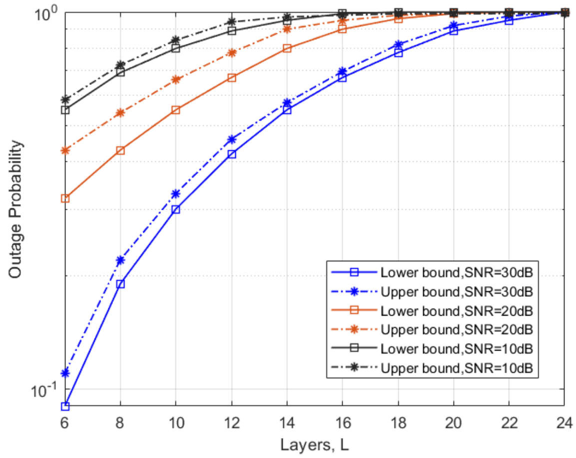

FIGURE 9. **Outage probability versus Layers for different SNR values.**

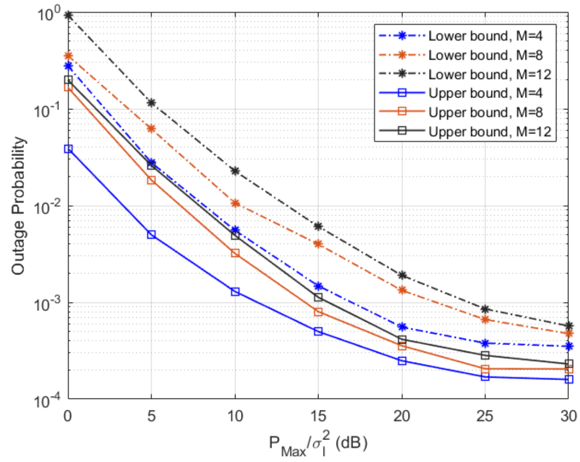

FIGURE 10. **Outage probability bounds variation with power ratio for different codebook sizes.**

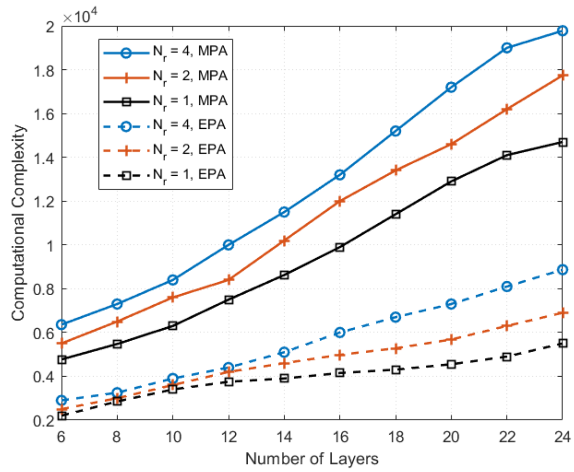

FIGURE 11. **Receiver complexity versus number of layers.**

Fig. 8 shows the system capacity performance versus channel estimation error, $e\Gamma_l$ for different number of layers considering a codebook size $M = 4$ and thus $N_t = 4$. It can be observed that the system capacity decreases sharply with deteriorating channel conditions i.e., as the channel error variance increases. Furthermore, M-PD-SCMA with $L = 24$ layers experience much degradation compared with $L = 16$ and $L = 12$ layers. As the number of layers increase, subsequently, the number of multiplexed users also multiplies resulting to escalated CSI imperfection from the additional noise terms. This scenario eventually leads to poor decoding experience especially with imperfect SIC where the error builds up. For enhanced performance, careful trade-off between CSI error variance and the number of layers is required.

Fig. 9 illustrates the upper and lower outage performances against number of layers deployed L at different SNR values. Additive deployment of layers subsequently increases the number of users transmitting in the system. There is substantial outage at low SNR values compared to high SNR values. The plots illustrates that the bounds are asymptotically tight for low and high SNR, respectively. Moreover, both bounds have identical slope for high SNR, which results in a close tunnel for the outage probability. As the number of layers increases, it becomes increasingly complex to decode both at MPA and SIC, therefore resulting to outage.

The outage bounds performance variation with power ratio at different codebook sizes M is presented in Fig. 10. As the ratio of maximum power P_{max} to the layer power increases, the outage reduces. The outage exhibited at higher power ratio is lower compared to low power ratio. The codebook size M also exhibits significant performance effect. The codebook size in this model corresponds to the number of codewords that can transmitted via spatial multiplexing and subsequently dictates the number of transmit antennas in play. At $M = 4$, both the upper and lower bounds experience reduced outage compared to $M = 6$ and $M = 12$ codebook sizes. Lower value of M across the layers provide power diversity advantage for the same P_{max} value thus providing SIC advantage in detecting the superimposed MUEs in a layer.

The computational complexity vs the number of SUEs or rather the number of layers employed for the proposed MUD algorithm is shown in Fig. 11. In this case we consider a fixed modulation order $M = 4$ and compare the EPA with MPA based MUDs complexity orders. It can be observed that the receiver MUD becomes more complex for both MPA and EPA as the value of L increases. This can be attributed to the increased number of VN indices connected to a single RN r_k. Predictably from the results, EPA based MUD exhibits significantly lower complexity order than MPA. Since only the means and variances of the messages are followed iteratively, EPA results in a linearly scaling complexity order unlike the exponential order resulting with MPA.

The overall system complexity versus the number of layers for different NOMA schemes is presented in Fig. 12. The total analyzed M-PD-SCMA complexity is the combinational complexity of the proposed RA schemes at the transmit-

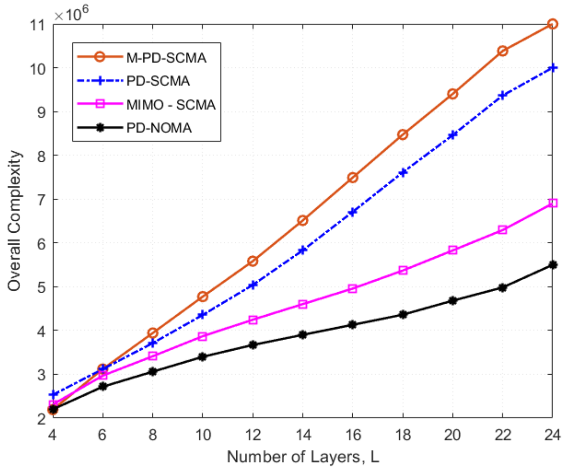

FIGURE 12. Computational complexity vs number of Layers for different NOMA schemes.

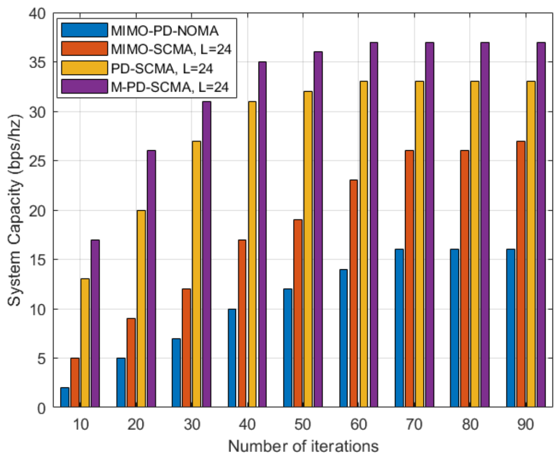

FIGURE 13. System convergence.

ter and joint MUD complexity at the receiver for all the N_r receive antennas. It is observed that the computational complexity increases with an increase in number of layers for all the NOMA schemes. Although M-PD-SCMA provides improved capacity, multiplexing and diversity gains, the implementation suffers increased complexity cost than PD-SCMA, MIMO-SCMA and PD-NOMA. The deployment of linearly complex EPA rather than exponentially complex MPA significantly reduces the computational complexity at the joint MUD. However, as the number of layers, transmit and receive antennas and multiplexed UEs increase, the overall complexity increase compoundingly.

Lastly, Fig. 13 shows the convergence behaviour of the multi-antenna PD-SCMA system compared with the PD-SCMA, SCMA and PD-NOMA. From the figure and considering decoding at each receive antenna, it can be deduced that after few iterations, system capacity converges. This reiterates the suitability of the proposed algorithms and validates the feasibility and practicability of the M-PD-SCMA system. Nonetheless, M-PD-SCMA employing multiple antenna schemes converge to an optimal solution with higher capacity compared to single antenna PD-SCMA system, MIMO-SCMA and MIMO-PD-NOMA.

VI. CONCLUSION

We have investigated the performance of spatial multiplexing uplink MIMO based hybrid power domain sparse code multiple access (M-PD-SCMA) system. To enhance performance at the receiver, a joint MUD based on modified EPA and SIC is proposed. The system's performance is analyzed based on parameters of capacity, BER, complexity and outage. Although the overall M-PD-SCMA system complexity surpasses other NOMA schemes, employing the modified EPA based MUD in the code-domain significantly reduces the complexity order compared to MPA. Hence, it is a good candidate MUD even as the number of antennas grow. Results show that M-PD-SCMA capacity benchmarks the PD-SCMA capacity and the BER and outage performance enhances with number of antennas and power diversity.

REFERENCES

[1] Y. Cai, Z. Qin, F. Cui, G. Y. Li, and J. A. McCann, "Modulation and multiple access for 5G networks," *IEEE Commun. Surveys Tuts.*, vol. 20, no. 1, pp. 629–646, 1st Quart., 2018.

[2] H. Nikopour and H. Baligh, "Sparse code multiple access," in *Proc. IEEE 24th Annu. Int. Symp. Pers., Indoor, Mobile Radio Commun. (PIMRC)*, Sep. 2013, pp. 332–336.

[3] C. Quan, A. Yadav, B. Geng, P. K. Varshney, and H. V. Poor, "A novel spectrally-efficient uplink hybrid-domain NOMA system," *IEEE Commun. Lett.*, vol. 24, no. 11, pp. 2609–2613, Nov. 2020.

[4] A. Bal, M. R. H. Khan, and M. K. Peyal, "Performance comparison among hybrid NOMA schemes focusing on outage performance and sum rate arrangement," in *Proc. 2nd Int. Conf. Emerg. Technol. (INCET)*, May 2021, pp. 1–5.

[5] M. Elbayoumi, W. Hamouda, and A. Youssef, "A hybrid NOMA/OMA scheme for MTC in ultra-dense networks," in *Proc. IEEE Global Commun. Conf. (GLOBECOM)*, Dec. 2020, pp. 1–6.

[6] M. Zeng, A. Yadav, O. A. Dobre, and H. V. Poor, "Energy-efficient joint user-RB association and power allocation for uplink hybrid NOMA-OMA," *IEEE Internet Things J.*, vol. 6, no. 3, pp. 5119–5131, Jun. 2019.

[7] S. Chege and T. Walingo, "Energy efficient resource allocation for uplink hybrid power domain sparse code nonorthogonal multiple access heterogeneous networks with statistical channel estimation," *Trans. Emerg. Telecommun. Technol.*, vol. 32, no. 1, p. e4185, Jan. 2021.

[8] S. Chege and T. Walingo, "Multiplexing capacity of hybrid PD-SCMA heterogeneous networks," *IEEE Trans. Veh. Technol.*, vol. 71, no. 6, pp. 6424–6438, Jun. 2022.

[9] S. Sharma, K. Deka, V. Bhatia, and A. Gupta, "Joint power-domain and SCMA-based NOMA system for downlink in 5G and beyond," *IEEE Commun. Let.*, vol. 23, no. 6, pp. 971–974, Jun. 2019.

[10] L. Lu, G. Y. Li, A. L. Swindlehurst, A. Ashikhmin, and R. Zhang, "An overview of massive MIMO: Benefits and challenges," *IEEE J. Sel. Topics Signal Process.*, vol. 8, no. 5, pp. 742–758, Jun. 2014.

[11] Y. Huang, C. Zhang, J. Wang, Y. Jing, L. Yang, and X. You, "Signal processing for MIMO-NOMA: Present and future challenges," *IEEE Wireless Commun.*, vol. 25, no. 2, pp. 32–38, Apr. 2018.

[12] M. Zeng, A. Yadav, O. A. Dobre, G. I. Tsiropoulos, and H. V. Poor, "Capacity comparison between MIMO-NOMA and MIMO-OMA with multiple users in a cluster," *IEEE J. Sel. Areas Commun.*, vol. 35, no. 10, pp. 2413–2424, Oct. 2017.

[13] Y. Chi, L. Liu, G. Song, C. Yuen, Y. L. Guan, and Y. Li, "Practical MIMO-NOMA: Low complexity and capacity-approaching solution," *IEEE Trans. Wireless Commun.*, vol. 17, no. 9, pp. 6251–6264, Sep. 2018.

[14] Z. Ding, L. Dai, and H. V. Poor, "MIMO-NOMA design for small packet transmission in the Internet of Things," *IEEE Access*, vol. 4, pp. 1393–1405, 2016.

[15] C. Chen, W.-De Zhong, H. Yang, and P. Du, "On the performance of MIMO-NOMA-based visible light communication systems," *IEEE Photon. Technol. Lett.*, vol. 30, no. 4, pp. 307–310, Feb. 15, 2018.
[16] Z. Mheich, I. A. Hemadeh, Z. Liu, and P. Xiao, "Low-complexity expectation propagation detection for uplink MIMO-SCMA systems," in *Proc. Int. Conf. U.K.-China Emerg. Technol. (UCET)*, Aug. 2020, pp. 1–4.
[17] S. Han, C. Guo, W. Meng, C. Li, Y. Cui, and W. Tang, "The uplink and downlink design of MIMO-SCMA system," in *Proc. Int. Wireless Commun. Mobile Comput. Conf. (IWCMC)*, Sep. 2016, pp. 56–60.
[18] W. Abdessamad, Y. Nasser, K. Y. Kabalan, and O. Bazzi, "On the performance evaluation of MIMO-SCMA systems," in *Proc. 8th Int. Congr. Ultra Modern Telecommun. Control Syst. Workshops (ICUMT)*, Oct. 2016, pp. 135–140.
[19] Z. Pan, J. Luo, J. Lei, L. Wen, and C. Tang, "Uplink spatial modulation SCMA system," *IEEE Commun. Lett.*, vol. 23, no. 1, pp. 184–187, Jan. 2018.
[20] Y. Du, B. Dong, Z. Chen, P. Gao, and J. Fang, "Joint sparse graph-detector design for downlink MIMO-SCMA systems," *IEEE Wireless Commun. Lett.*, vol. 6, no. 1, pp. 14–17, Feb. 2016.
[21] S. Tang, L. Hao, and Z. Ma, "Low complexity joint MPA detection for downlink MIMO-SCMA," in *Proc. IEEE Global Commun. Conf. (GLOBECOM)*, Dec. 2016, pp. 1–4.
[22] V. A. Mardinata, D. Kurniawan, and N. Armi, "Impact of overloading factor on MIMO–SCMA systems," in *Proc. Int. Conf. Radar, Antenna, Microw., Electron., Telecommun. (ICRAMET)*, Nov. 2021, pp. 95–98.
[23] A. Yadav, C. Quan, P. K. Varshney, and H. V. Poor, "On performance comparison of multi-antenna HD-NOMA, SCMA, and PD-NOMA schemes," *IEEE Wireless Commun. Lett.*, vol. 10, no. 4, pp. 715–719, Apr. 2021.
[24] Z. Wu, C. Zhang, X. Shen, and H. Jiao, "Low complexity uplink SFBC-based MIMO-SCMA joint decoding algorithm," in *Proc. 3rd IEEE Int. Conf. Comput. Commun. (ICCC)*, Dec. 2017, pp. 968–972.
[25] J. Dai, G. Chen, K. Niu, and J. Lin, "Partially active message passing receiver for MIMO-SCMA systems," *IEEE Wireless Commun. Lett.*, vol. 7, no. 2, pp. 222–225, Apr. 2017.
[26] A. Kosasih, O. Setyawati, and R. Rahmadwati, "Low complexity multi-user MIMO detection for uplink SCMA system using expectation propagation algorithm," *Telkomnika*, vol. 16, no. 1, pp. 182–188, 2018.
[27] X. Meng, Y. Wu, Y. Chen, and M. Cheng, "Low complexity receiver for uplink SCMA system via expectation propagation," in *Proc. IEEE Wireless Commun. Netw. Conf. (WCNC)*, Mar. 2017, pp. 1–5.
[28] T. P. Minka, "Expectation propagation for approximate Bayesian inference," 2013, *arXiv:1301.2294*.
[29] P. Wang, L. Liu, S. Zhou, G. Peng, S. Yin, and S. Wei, "Near-optimal MIMO-SCMA uplink detection with low-complexity expectation propagation," *IEEE Trans. Wireless Commun.*, vol. 19, no. 2, pp. 1025–1037, Feb. 2019.
[30] M. Vaezi and H. V. Poor, *NOMA: An Information-Theoretic Perspective*. Cham, Switzerland: Springer, 2019, pp. 167–193.
[31] T. Sefako and T. Walingo, "Biological resource allocation algorithms for heterogeneous uplink PD-SCMA NOMA networks," *IEEE Access*, vol. 8, pp. 194950–194963, 2020.
[32] J. Wang, B. Xia, K. Xiao, Y. Gao, and S. Ma, "Outage performance analysis for wireless non-orthogonal multiple access systems," *IEEE Access*, vol. 6, pp. 3611–3618, 2018.
[33] W. B. Ameur, P. Mary, M. Dumay, J.-F. Helard, and J. Schwoerer, "Performance study of MPA, LOG-MPA and MAX-Log-MPA for an uplink SCMA scenario," in *Proc. 26th Int. Conf. Telecommun. (ICT)*, 2019, pp. 411–416.
[34] X. Meng, S. Wu, L. Kuang, Z. Ni, and J. Lu, "Expectation propagation based iterative multi-user detection for MIMO-IDMA systems," in *Proc. IEEE 79th Veh. Technol. Conf. (VTC Spring)*, May 2014, pp. 1–5.
[35] C. Wang, E. K. S. Au, R. D. Murch, W. H. Mow, R. S. Cheng, and V. Lau, "On the performance of the MIMO zero-forcing receiver in the presence of channel estimation error," *IEEE Trans. Wireless Commun.*, vol. 6, no. 3, pp. 805–810, Mar. 2007.
[36] B. Zerlin, J. Brehmer, and J. Nossek, "On the channel outage probability of multi-user CDMA systems," in *Proc. IEEE 16th Int. Symp. Personal, Indoor Mobile Radio Commun.*, vol. 3, Sep. 2005, pp. 1510–1514.

SIMON CHEGE (Member, IEEE) received the B.Sc. degree in electrical and communications engineering from Moi University, Kenya, the M.Sc. degree in electrical and electronic engineering from JNTU–Anantapur, India, and the Ph.D. degree in electronic engineering from the University of KwaZulu Natal, Durban, South Africa. His current research interests include wireless communications and multiple access technologies.

TOM WALINGO (Member, IEEE) received the B.Sc. degree in electrical and communications engineering from Moi University, Kenya, the M.Sc. degree in electronic engineering from the University of Natal, and the Ph.D. degree in electronic engineering from the University of KwaZulu–Natal, Durban, South Africa. He is currently a Researcher with the Center of Radio Access and Rural Technology and a Professor in communications and computer engineering at the University of KwaZulu–Natal. He has authored many peer-reviewed journals and conference papers. His current research interests include digital and wireless communications, satellite communications, and wireless sensor networks. He was a recipient of several research awards, including the SAIEE ARJ 2013 Award. He is an editor/reviewer of several journals in his field.